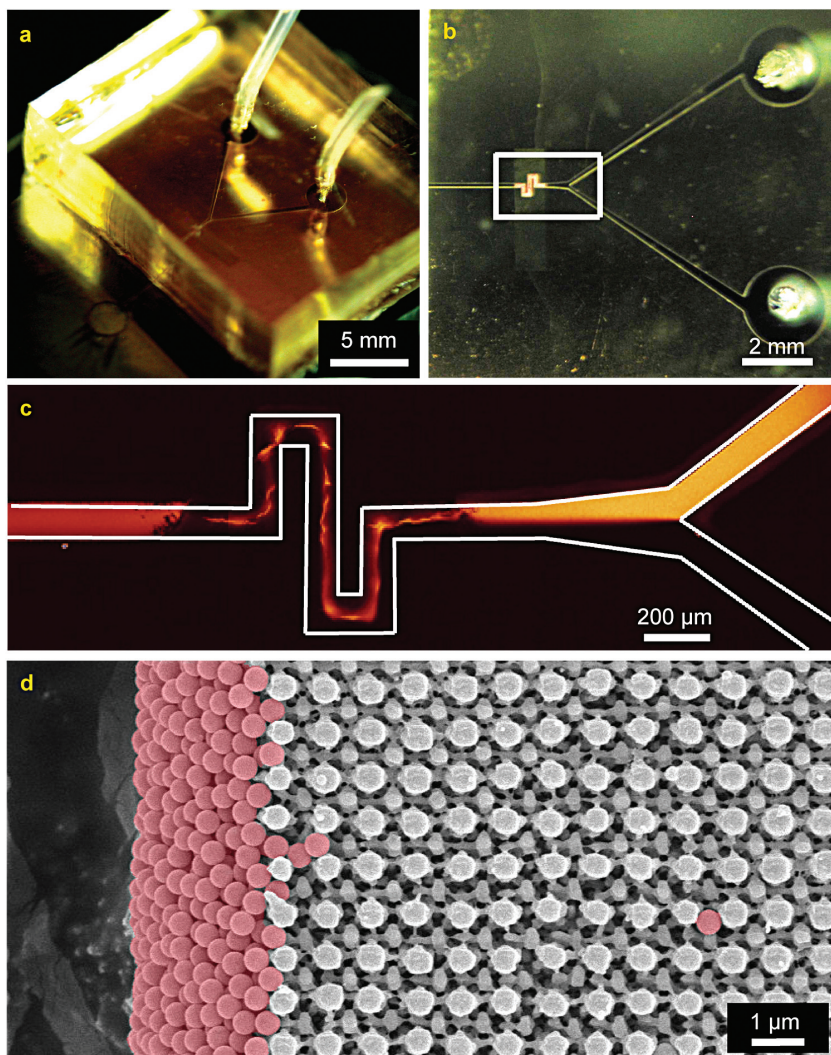


VOLUME 111
NOVEMBER 15, 2007
NUMBER 45
<http://pubs.acs.org/JPCB>

THE JOURNAL OF PHYSICAL CHEMISTRY

B

**Three-Dimensional
Nanostructures
Formed by
Conformable Phase
Mask Lithography,
with Applications
in Microfluidics
(see page XXX)**



CONDENSED MATTER AND BIOPHYSICAL CHEMISTRY

PUBLISHED WEEKLY BY THE AMERICAN CHEMICAL SOCIETY



FEATURE ARTICLE

Three-Dimensional Nanofabrication with Elastomeric Phase Masks

Daniel J. Shir,[†] Seokwoo Jeon,[†] Hongwei Liao,[†] Matthew Highland,[†] David G. Cahill,[†] Mehmet F. Su,[‡] Ihab F. El-Kady,^{‡,§} Christos G. Christodoulou,[‡] Gregory R. Bogart,[§] Alex V. Hamza,[#] and John A. Rogers^{*,‡}

Department of Materials Science and Engineering and Seitz Materials Research Laboratory, University of Illinois, Urbana, Illinois 61801, Department of Electrical and Computer Engineering, University of New Mexico, Albuquerque, New Mexico 87131, Sandia National Laboratory, Albuquerque, New Mexico 87185, and Lawrence Livermore National Laboratory, Livermore, California

Received: May 27, 2007

This Feature Article reviews recent work on an optical technique for fabricating, in a single exposure step, three-dimensional (3D) nanostructures with diverse structural layouts. The approach, which we refer to as proximity field nanopatterning, uses conformable, elastomeric phase masks to pattern thick layers of transparent, photosensitive materials in a conformal contact mode geometry. Aspects of the optics, the materials, and the physical chemistry associated with this method are outlined. A range of 3D structures illustrate its capabilities, and several application examples demonstrate possible areas of use in technologies ranging from microfluidics to photonic materials to density gradient structures for chemical release and high-energy density science.

1. Introduction

Capabilities for fabricating three-dimensional (3D) nanostructures are important for many areas of technology including microfluidics,^{1–3} sensors,⁴ photonics,^{5–7} electrodes in fuel cells,⁸ catalyst carriers,^{9,10} data storage,^{11,12} and many others. The most widespread approach for forming such structures relies on sequential, repeated applications of primarily two-dimensional (2D) patterning techniques, such as photolithography^{13,14} and electron beam lithography,^{13,14} followed by selective removal of sacrificial resist materials. The high levels of engineering sophistication and the deep, basic physical understanding of these 2D approaches lead to extremely powerful manufacturing platforms for certain established devices in electronics and photonics. Their application to 3D structures, however, is difficult due to the layer-by-layer strategies that are required. As a result, many groups have explored alternative, unconventional techniques that can form 3D nanostructures more conveniently. Those techniques include approaches based on colloidal self-assembly,^{9,15–18} phase separation of polymers,^{19–21} template-controlled growth,^{22,23} self-assembly in fluids,^{24,25} holographic based lithography,^{26–29} controlled chemical etching,^{30,31} direct-write techniques based on multiphoton exposures^{11,32,33} and filamentary inks,^{7,34} and many others. Each of these techniques provides important capabilities for fabricating various classes of 3D structures that would be difficult or impossible to produce effectively using established methods. Nevertheless, none provides a complete solution to the challenge of 3D nanofabrication, due to various combinations of disadvantages that include limited flexibility in the structure geom-

etries, slow speeds, applicability only to relatively small areas, complex experimental setups, and uncertain yields and defect densities. Our recent work, summarized in this Feature Article, seeks to establish a different approach to 3D nanofabrication that avoids some of these problems. The goal is to establish patterning capabilities that complement other methods in a way that can enable certain important applications. The technique involves single or multiphoton exposure of thick, transparent photosensitive materials through soft, elastomeric subwavelength phase masks in conformal contact mode geometries.^{35–41} We refer to this method as proximity field nanopatterning (PnP), due to its use of optical effects that occur in proximity to the masking element. This Feature Article provides an overview of the process, with discussions of key aspects of the associated optics, physical chemistry and materials science. Diverse classes of periodic, aperiodic, and even quasi-crystalline 3D nanostructures demonstrate some of the patterning capabilities, with application examples in microfluidics, photonics, high-energy density science, chemical release and others.

2. Proximity Field Nanopatterning

2.1. Overview of Approach. The PnP process³⁵ involves three components: (i) a light source, which determines the wavelength, the intensity, and the angular and spectral bandwidth for the photoexposure, (ii) a soft, elastomeric phase mask, which represents all of the necessary optics, and (iii) a photosensitive material capable of forming a solid structure in the geometry of the 3D distribution of intensity created by passing exposure light through the mask. Figure 1 contains a diagram outlining the steps. The process begins with casting of a layer of the photosensitive material onto a substrate. This layer is typically a solid film, although backside exposures²² or specialized masks enable the use of liquids. Next, placing the elastomeric phase mask against the film leads to atomic scale, conformal contact due to the action of generalized adhesion

* Corresponding author. E-mail: jrogers@uiuc.edu.

[†] University of Illinois.

[‡] University of New Mexico.

[§] Sandia National Laboratory.

[#] Lawrence Livermore National Laboratory.



Daniel Shir received his B.S. degree from Pennsylvania State University in Materials Science and Engineering in 2005. He is currently pursuing a Ph.D. degree in materials science and engineering at the University of Illinois at Urbana-Champaign under Professor John A. Rogers' guidance. His research interests include soft lithography, 3D nanostructures, novel fabrication techniques, photonic crystals, and unusual optical devices.



Seokwoo Jeon was born in Seoul, Korea, in 1975. He received his B.S. degree in 2000 and his Master degree with Professor Shinho Kang from Seoul National University in 2003 after a one-year exchange graduate program with Professor Paul V. Braun at the University of Illinois at Urbana-Champaign (UIUC). He got his Ph.D. in Materials Science and Engineering at UIUC under the guidance of Professor John A. Rogers. Working as a postdoctoral research scientist at Nanoscale Science and Engineering Center at Columbia University with Prof. Colin Nuckolls, Prof. James Hone, and Prof. Philip Kim, he investigates nanoelectronic materials. Research interests include soft lithography, 3D nanopatterning, microfluidic systems, low-dimensional nanoelectronics, and optically functional materials & devices.

Hongwei Liao received B.S. and M.S. degrees in chemistry from the University of Science and Technology of China (USTC) in 1998 and 2001, respectively. In 2006, he was awarded a Ph.D. degree in physical chemistry from Rice University under the guidance of Professor Jason Hafner. His research interests include 3D nanostructures. He is currently a postdoctoral fellow in Professor John Rogers' group in the Department of Materials Science and Engineering at the University of Illinois at Urbana-Champaign. His research interests include soft lithography, transfer printing, and photonic structures and devices.

Matthew Highland received his B.A. in physics from Illinois Wesleyan University in 2002 and his Ph.D. in physics from North Carolina State University in 2006. He is currently a postdoctoral researcher in the Materials Science department at the University of Illinois with Dr. David Cahill's group, studying thermal properties of nanoscale systems.

forces (primarily van der Waals interactions)^{42–44} without external application of pressure. The mask has structures of surface relief that modulate the phase of transmitted light by a magnitude and in a spatial geometry defined by the layout and depth of the relief, and by the index of refraction of the elastomer. This spatial phase modulation creates a 3D distribution of intensity that patterns the exposure of the photosensitive



David Cahill is a professor of Materials Science and Willett Professor of Engineering at the University of Illinois in Urbana. David received his Ph.D. in condensed matter physics from Cornell University in 1989 and worked as a postdoctoral research associate at IBM Watson Research Center before joining the faculty of the U. of Illinois in 1991. David's current research includes thermal transport at the nanoscale, thermodynamics of aqueous interfaces, ultrafast and strongly-driven transformations in materials, and the development of new experimental tools for the measurement of thermophysical properties.

Mehmet F. Su received his M.S. degree in computer engineering from University of New Mexico in 2006. He is continuing his studies as a Ph.D. candidate in the Electrical and Computer Engineering Department at UNM. Mr. Su is the author/co-author of more than 14 publications in the fields of photonic and phononic crystal research. His research interests include photonic and phononic crystal applications, numerical methods in computational electromagnetics, and high-performance computing applications in scientific simulations.

Ihab F. El-Kady. Information not available.

Christos G. Christodoulou received his Ph.D. degree in Electrical Engineering from North Carolina State University in 1985. He is a professor in the Electrical and Computer Engineering Department of the University of New Mexico. He is a Fellow member of IEEE and a member of Commission B of USNC/URSI, Eta Kappa Nu, and the Electromagnetics Academy. He was appointed as an IEEE AP-S Distinguished Lecturer for 2007–2009. He has published over 270 papers in journals and conference proceedings, has 12 book chapters, and has co-authored 4 books.



Gregory R. Bogart received his B.S. degree in chemistry from St. Cloud State University in St. Cloud, MN, and his Ph.D. in chemistry from Colorado State University in Fort Collins, CO. His research interests involve development and transferring to manufacturing new technologies. He holds 12 U.S. patents and is currently employed at Symphony Acoustics in Rio Rancho, NM, where he is Vice President of Engineering.

layer in the region next to the mask. This intensity distribution extends from the near surface region of the mask (i.e., within a wavelength; the near field region) to distances of many wavelengths (i.e., the region in proximity to the surface of the



Alex V. Hamza did his Bachelor's and Master's work at MIT in 1981 and his Ph.D. work at Stanford University in 1986, all in Chemical Engineering. He was an Alexander von Humboldt Fellow at the Fritz-Haber-Intstute of the Max-Planck-Gesellschaft in 1987. His research interests are in surface and interface science and nanoscale synthesis and characterization. He is currently the Director of the Nanoscale Synthesis and Characterization Laboratory at Lawrence Livermore National Laboratory.



John A. Rogers obtained BA and BS degrees in chemistry and in physics from the University of Texas, Austin, in 1989. From MIT, he received SM degrees in physics and in chemistry in 1992 and the Ph.D. degree in physical chemistry in 1995. From 1995 to 1997, Rogers was a Junior Fellow in the Harvard University Society of Fellows. During this time he also served as a Director for Active Impulse Systems, a company based on his Ph.D. research that he co-founded in 1995 and which was acquired by a large company in 1998. He joined Bell Laboratories as a Member of Technical Staff in the Condensed Matter Physics Research Department in 1997 and served as Director of this department from 2000 to 2002. He is currently Founder Professor of Engineering at University of Illinois at Urbana-Champaign, with appointments in the Departments of Materials Science and Engineering, Electrical and Computer Engineering, Mechanical Science, and Engineering and Chemistry. Rogers research includes fundamental and applied aspects of nanoscale and molecular scale fabrication, materials and patterning techniques for large area electronics, and unusual photonic systems.

mask) and up to several millimeters away, limited only by the size of the mask and the diameter and coherence of the exposure source. Removing the mask following this exposure, and then developing away the regions of photosensitive material that were (or were not, depending on the chemistry) exposed to light completes the fabrication.³⁵ The 3D structures formed in this way can be used directly in applications or they can template the deposition or growth of other materials.

The soft, elastomeric phase mask represents an unusual type of optical element that is central to the PnP method. These masks can be formed easily by casting and curing liquid prepolymers against suitable structures of relief, known as "masters", using

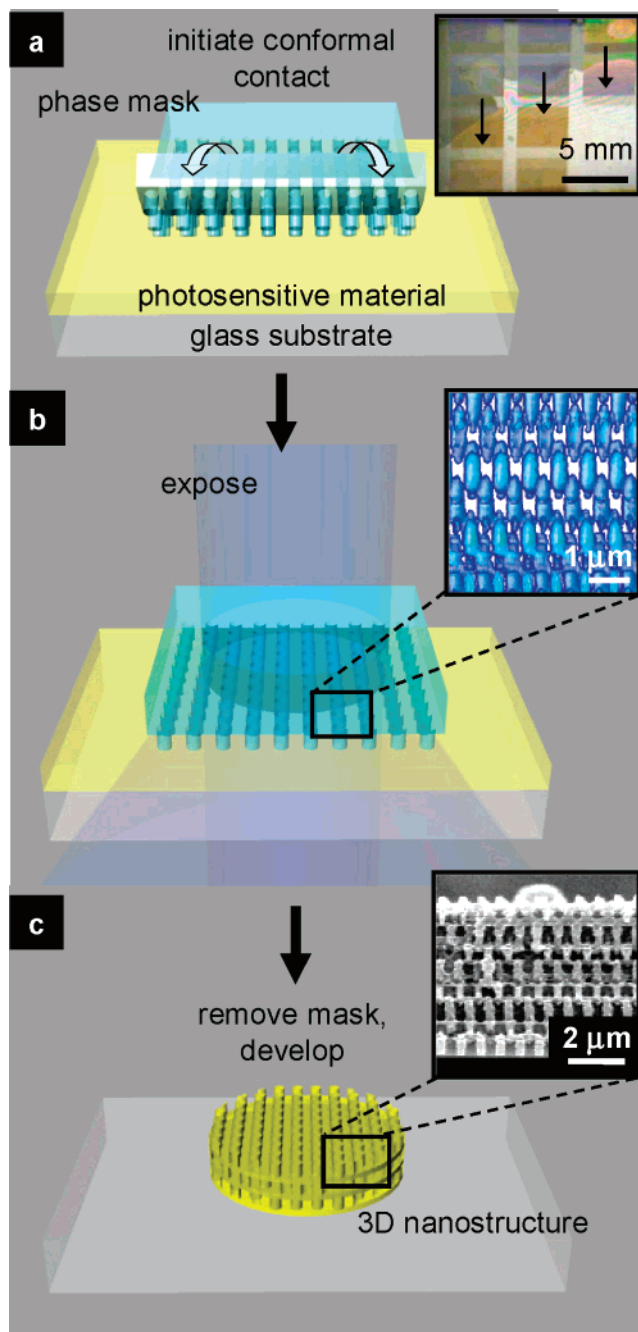


Figure 1. Schematic illustration of process steps for a procedure, referred to as proximity field nanopatterning (PnP), that uses high-resolution conformable, elastomeric phase masks to produce three-dimensional (3D) nanostructures. (a) Placing such a mask on the surface of a solid film of a transparent, photosensitive material leads to intimate, conformal contact driven by generalized forces, without applied pressure. The inset shows an optical image of the phase mask as it establishes such contact. (b) Passing light through the mask generates a complex intensity distribution throughout the thickness of the film. The inset shows a 3D rendering of the intensity measured by near field scanning optical microscopy for the case of a mask that has relief features in the geometry of a square array of cylindrical posts with diameters of 375 nm, heights of 420 nm, and periodicity of 566 nm. (c) Washing away the parts of the photosensitive material that were (or were not, depending on the chemistry) exposed yields a 3D nanostructure. The inset shows a scanning electron micrograph of a typical example.

the techniques of soft lithography.^{35,45,46} The polymers are typically commercially available elastomers based on polydimethylsiloxanes (PDMS; Sylgard 184, Dow Corning)^{45–48} or perfluoropolyethers (PFPE; CN4000, Sartomer Co., Inc.).^{49,50}

These materials are useful due to their optical transparency down to wavelengths of $\sim 250\text{--}300$ nm and their ability to replicate accurately features of relief in the “masters” with dimensions down to ~ 1 nm^{51–53}. Also, their moderate to low Young’s moduli (i.e., between 1 and 10 MPa)^{45,50} enable soft, conformal contact of the mask with the photosensitive layer and, therefore, repeatable alignment of the optical element with respect to the photopolymer surface to nanometer precision without the use of elaborate staging systems, as demonstrated previously with these types of mask in two-dimensional photopatterning methods.^{54–56} This type of reversible and nondestructive physical contact has other important features. In particular, it provides (i) a continuous, gap-free optical coupling between the mask and photosensitive layer, thereby enabling the regions in proximity to the mask to be used reliably for optical patterning, (ii) simple experimental setups in which additional position control systems (for the out of plane direction) and optical elements (i.e., imaging lenses, etc) are not required, (iii) an insensitivity to acoustic or mechanical vibrations during optical exposure, due to the physical contact between the mask and photosensitive material, (iv) relaxed requirements on the coherence of the exposure source due to the proximity geometry, thereby enabling 3D patterning even with incoherent light from a lamp, and (v) the ability to exploit either single or multiphoton effects for patterning, using the same setups with suitable light sources.

These features lead to levels of patterning flexibility and experimental simplicity that make PnP attractive for many applications. In particular, various schemes for performing PnP enable structures with unusual directionality³⁸ and spatial gradients in feature sizes,^{39,40} in simple or complex geometries ranging from purely periodic to completely aperiodic layouts and many possibilities in between, including even quasicrystalline arrangements.^{35–41} As summarized in this paper, we have experimentally demonstrated many of these capabilities and explored the use of PnP for various applications in microfluidics (passive mixers and filters),^{35,37} photonics (photonic band gap, PBG, materials),⁴¹ high-energy density science (reservoir targets for shockless laser compression),⁵⁷ and chemical/drug release scaffolds.⁴⁰ These and other aspects are summarized following descriptions of the optics, masks and photosensitive materials.

2.2. Optics. The complex 3D intensity distributions that form upon passage of light through the phase masks can be understood by first considering the simplest case of monochromatic plane waves and masks that consist of parallel raised and recessed regions of relief, in the geometry of a line grating. Such a setup exhibits characteristics of a well-known optical phenomenon called the Talbot effect, or self-imaging^{58–60} effect. Here, an image (i.e., distribution of intensity) that forms at any given distance from the surface of the mask repeats, or recurs, at an integer multiple of the Talbot distance away from the mask surface. The Talbot distance, Z_T , is given by^{58–61}

$$Z_T = \frac{\lambda}{1 - (1 - \lambda^2/p^2)^{0.5}} \cong \frac{2p^2}{\lambda} \quad (\text{when } \lambda/p \text{ is small}) \quad (1)$$

where λ is the wavelength of light in the media it propagates and p is the periodicity of the grating. Although the details of the distributions of intensity depend on many factors that do not appear explicitly in eq 1, this simple Talbot effect, and related phenomena such as the fractional Talbot effect,⁶¹ explain the periodicity and basic features of the variations in intensity with distance from the surface of the mask.

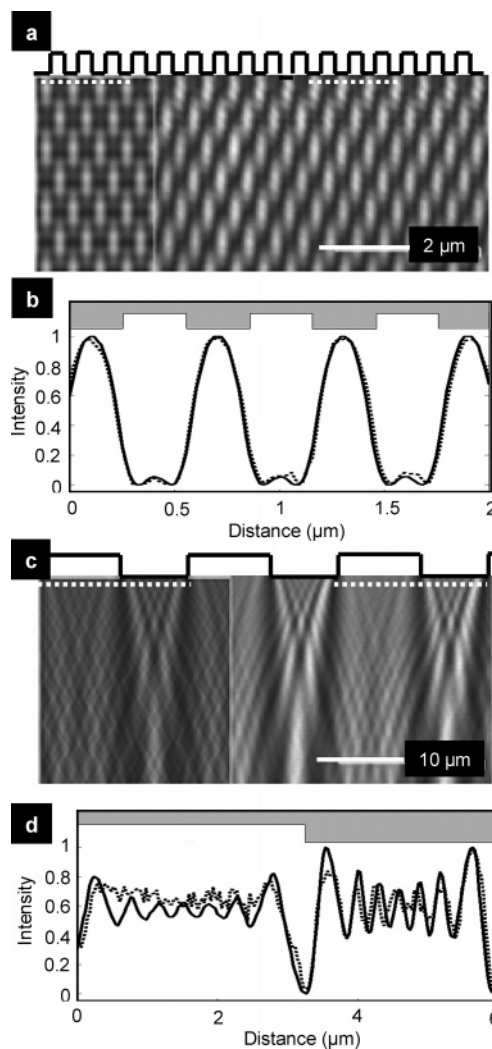


Figure 2. Near field optical measurements and simulations (left hand parts of (a) and (c); lines in (b) and (d)) of the propagation of laser light (442 nm, TM polarization; HeCd) through line grating, surface relief phase masks with different periodicities. Schematic layouts of the masks appear at the tops of the graphs and images. (a) and (c) images for masks with line widths and spacings of 300 nm and of 4.4 and 5.6 μm , respectively. (b) and (d) line cuts of the simulations (full line) and measurements (dashed line) for (a) and (c), respectively, evaluated at positions indicated by the dashed lines in these frames.

The Talbot effect can be observed clearly through direct measurements of the distributions of intensity with a near field scanning optical microscope (NSOM; WITec, Inc). Figure 2a shows such results for a line grating mask with $p = 600$ nm and a relief depth (RD) of 330 nm when illuminated with a HeCd laser at a wavelength of 442 nm.⁵⁶ The lateral dimensions of the lines in this grating are smaller than the incident wavelength, which leads to a type of effective subwavelength focusing that creates high- and low-intensity regions near the surface of the mask at the raised and recessed features of relief, respectively. This image repeats, consistent with the Talbot effect and eq 1, at distances equal to integer multiples of 1365 nm. Figure 2b provides linecuts from the NSOM measurements (dashed line) in Figure 2a. Finite element modeling (FEM) (FEMLab, Comsol, Inc.) of the optics quantitatively reproduces these observations, as illustrated in Figure 2a (left inset) and 2b (solid line).⁵⁶ The situation is more complex for line grating masks with larger periods. As an example, parts c and d of Figure 2 show measurements and modeling for a mask with $p = 10 \mu\text{m}$ and $\text{RD} = 1.42 \mu\text{m}$. In this case, the Talbot distance

is $\sim 450 \mu\text{m}$, which is sufficiently large that only the fractional Talbot planes appear within the field of view of Figure 2. As for the case of the short period grating, FEM modeling quantitatively captures all of the details of the experimental observations.⁵⁶

The Abbe theory of image formation⁶² provides an alternative view of the optics.³⁵ In this picture, the masks create multiple beams of light by diffraction. Although spatially separated in the far field regime, these beams overlap and coherently interfere in the region near the mask to produce the distributions of intensity that are involved in the exposure. For the case of the short period mask of Figure 2a, only three diffracted beams (i.e., the 0th, +1st, and -1st orders) appear in the far field; the interference of these three beams leads to the relatively simple patterns illustrated in Figure 2a,b. The long period mask of Figure 2c, by contrast, generates 45 diffracted beams whose overlap creates a complex distribution with a corresponding number of spatial Fourier components. A computational approach based on the Abbe picture can complement the FEM technique mentioned previously. Such calculations involve determining the angles, intensities, phases, and polarization states of beams produced by far field diffraction and then computing the interference patterns that result from overlap of these beams. This approach reproduces the observed patterns, consistent with FEM, but in a more computationally efficient manner.^{35,56} Disadvantages include a neglect of near field effects (rarely important for PnP), and a limited ability to compute results efficiently for aperiodic or quasicrystal phase masks where the numbers of diffracted beams can be very large.

The Abbe method is extremely well suited for masks that consist of two-dimensional repeating structures of relief. Rigorous coupled wave analysis (RCWA) (Gsolver, Grating Solver Development Co.) yields the far field diffraction patterns, and separate codes determine the patterns of intensity that result from overlapping the diffracted beams.³⁵ Simulations and measurements corresponding to a phase mask that consists of a square array of posts (diameter, $d = 1000 \text{ nm}$, $\text{RD} = 420 \text{ nm}$, and $p = 1570 \text{ nm}$) provides an example of this approach. Figure 3 (top frame) illustrates a 3D rendering in the form of a solid structure that results from the application of a cutoff filter to the intensity distribution.³⁸ The bottom frames in Figure 3 provide a comparison between simulation and NSOM results at different distances from the mask, illustrating a good level of agreement.³⁸

2.3. Elastomeric Phase Masks. PnP relies on high-quality phase masks that are simple to fabricate and capable of achieving the necessary conformal contact. Transparent elastomers of the type that have been traditionally used for soft lithography^{45–46} are attractive for this purpose because optimized materials can reproduce, through casting and curing processes, relief structures on a “master” with fidelity down to the single nanometer range.^{50–53} Furthermore, this casting and curing process can be repeated many times with a single “master” to create many high-quality phase masks, each of which can be used multiple times. The “masters” for PnP typically consist of patterns of photoresist formed by deep ultraviolet projection mode photolithography.³⁵ The resulting masks involve a single depth of relief across their entire surfaces and are referred to as binary phase masks. Multilevel masks can be created either by stacking separate binary masks or by using multilevel masters. The thickness of the photoresist defines the depth of relief on a binary mask. This relief is often chosen such that the phase of the transmitted light is modulated by a substantial fraction of π . For typical

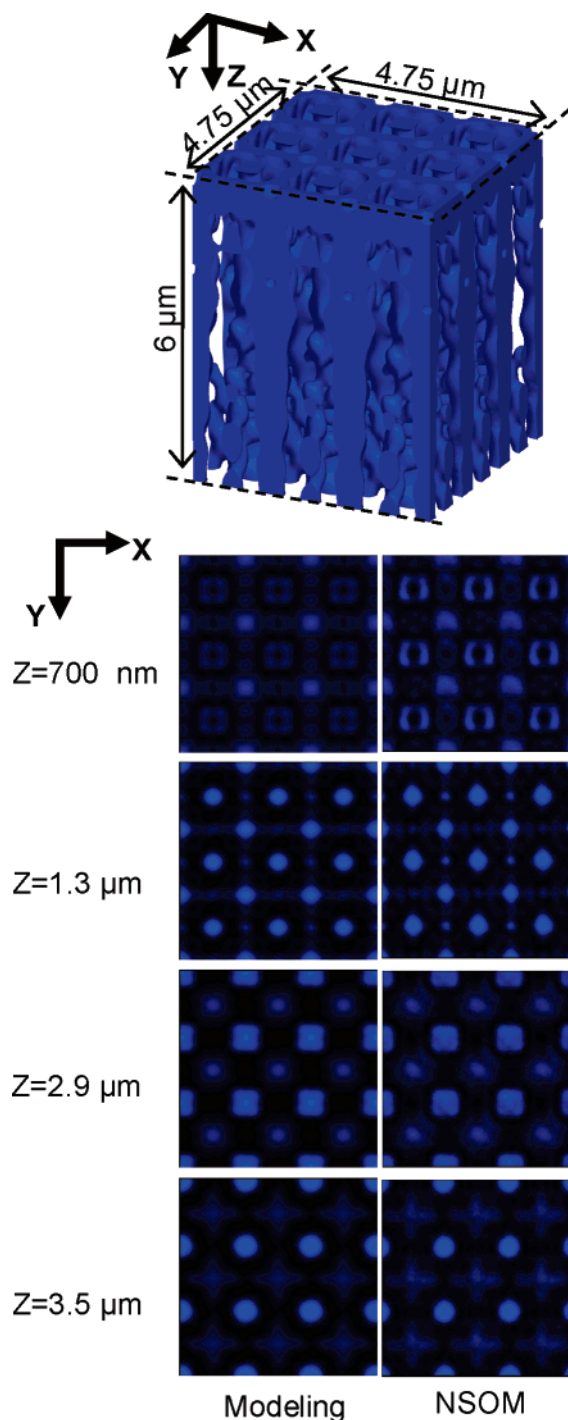


Figure 3. Simulations and measurements of 3D distributions of intensity formed by passage of 442 nm laser light (HeCd) through a phase mask (polyurethane; refractive index of 1.56) that consists of a square array of round holes ($d = 1000 \text{ nm}$, $\text{RD} = 420 \text{ nm}$, $p = 1570 \text{ nm}$). (Top frame) solid rendering of the simulated distribution, created by application of a cutoff filter to the data. (Bottom frame) simulated (left) and measured (right) intensity distributions evaluated at different distances (z) from the surface of the mask.

mask materials, this depth corresponds to a distance on the order of one wavelength of the exposure light.

Most of our work involves binary masks made of elastomers based on silicones or perfluoropolyethers. The silicones include variants of polydimethylsiloxane (PDMS) that yield low- ($\sim 2 \text{ MPa}$) and comparatively-high-modulus ($\sim 10 \text{ MPa}$) materials, which we refer to as s-PDMS and h-PDMS, respectively.^{45,47–48} These PDMS materials are attractive because they have (i) very

low surface energies (~ 25 mN/m)^{45,47} and low Young's moduli (1–10 MPa),^{45,47} which allow reversible, nondestructive conformal contact to flat surfaces without applied pressure, via the action of generalized adhesion forces,^{42–44} (ii) the ability to replicate surface relief structures with high fidelity,^{51–52} (iii) high physical toughness,^{49–50} making them robust to repeated use, and (iv) low-cost, commercial sources of material, thereby simplifying development work. Many of these same features make PDMS attractive for stamps and molds in traditional soft lithographic methods. h-PDMS provides capabilities for better resolution and higher aspect ratio features of relief compared to s-PDMS.^{47–48} Because this material is brittle, however, its implementation in a phase mask is most effective as a thin layer with a thick backing of the s-PDMS to facilitate handling.^{35,48,63} In-plane distortions, created during fabrication or use, can be reduced by the use of rigid backing layers in place of the s-PDMS.^{48,63}

Perfluoropolyethers (PFPEs) offer certain advantages compared to PDMS for soft lithography, including (i) lower surface energy,^{49,50} (ii) compatibility with organic solvents,^{49,64,65} and (iii) the ability to produce finer features with higher aspect ratios.^{49,50,66} These features can also be beneficial for PnP. We recently reported the use of a commercially available acryloxy perfluoropolyether, which we refer to as a-PFPE, for PnP and soft lithographic methods.⁵⁰ Compared to PDMS masks, the a-PFPE masks typically have fewer defects than those made with PDMS at certain challenging feature dimensions that are important for PnP.⁵⁰ The mechanical fragility of the a-PFPE is comparable to or slightly worse than h-PDMS. Although chemically bonding a backing layer of a more physically tough elastomer (e.g., s-PDMS) to PFPEs can be difficult, we find that phase masks consisting of thin layers of a-PFPE physically adhered to supports of s-PDMS can be sufficiently robust for routine use.⁵⁰ One minor disadvantage of using PFPE is its somewhat lower index of refraction (~ 1.35) compared to PDMS (~ 1.4), which demands slightly larger depths of relief to achieve comparable modulations in phase.

2.4. Photosensitive Material. The photosensitive materials act as a recording media to capture, in the form of solid structures, the 3D intensity distributions near the surface of the masks. The physical and chemical properties of these materials play important roles in the PnP process. In particular, the photosensitivity, the contrast, the index of refraction, and the diffusion of photocatalysts affect the resolution. The index of refraction can influence the number of spatial Fourier components associated with the structures; it also affects the Talbot distance and, as a result, the periodicity in the out-of-plane direction. The mechanical properties determine the robustness and strength of the 3D structures, and therefore their ability to withstand the capillary forces that can be associated with drying after the development as well as stresses that can occur in applications or subsequent processing (e.g., templated deposition or growth of other materials). In addition, other properties such as absorption length, wavelength sensitivity, and two-photon or three-photon absorption cross sections all can be exploited to achieve various capabilities in PnP, as described in subsequent sections.

Most of the structures reported in this Feature Article used a commercial epoxy-based photosensitive material (SU-8, MicroChem, Inc.).^{66,67} The SU-8 is a negative tone, cationic type of photoresist that offers high sensitivity, high resolution, and good transparency from the near-infrared (IR) to the visible and the near-ultraviolet (UV) range, with good structural properties, and usable levels of two-photon sensitivity.^{67–69} The material

consists of EPON SU-8 resin (Shell Chemical), a photosensitizer (propylene carbonate), and a photoacid generator (onium salt) dissolved in a solvent (γ -butyrolactone). The photosensitizer in SU-8 is sensitive to wavelengths less than 400 nm, but the absorption of the monomer is significant below 350 nm.⁷⁰ The range of useful exposure wavelengths for implementation of PnP with one-photon effects in this material is, therefore, between 400 and 350 nm. The incorporation of alternative photosensitizers and photoacid generators enables sensitivity in the visible, which can be useful in certain cases.⁷¹ The photochemical process involves optical absorption by the photosensitizer, which leads to the transfer of an electron to the photoacid generator. This acid, upon thermal treatment, promotes a cationic chain reaction that opens one of eight ring structures in the epoxy groups of the monomer for cross-linking.^{67,72,73} The amplification provided by the chain reaction enables sufficiently low concentrations of acid that the optical properties are unaffected, thereby causing negligible impact on the 3D imaging. The main disadvantages of SU8 for PnP include limited thermal stability, large levels of dimensional change that can occur during development or use, and relatively low mechanical toughness.

Other photosensitive materials such as poly(methylsilsesquioxanes) (PMSSQs)^{74–76} and certain chalcogenides^{76–78} can also be used in PnP. PMSSQ is attractive in part because its high thermal stability allows high-temperature processing, thereby enabling its use as a template, for example, in chemical vapor deposition processes at up to ~ 500 °C.^{74,76} Chalcogenide glasses are interesting, in part, because their high refractive index (2.35–3.5) leads to the possibility for direct patterning of PBG structures. Their high densities (3.2–6.35 g/cm³, depending on materials composition) can also be useful because they enable the formation of large gradients in effective density in nanoporous structures, which is important for certain applications discussed in a following section.

3. Patterning Capabilities

Wide ranging classes of 3D structures can be formed with PnP. The following sections provide examples achieved with different phase masks, with one- and two-photon processes, controlled levels of angular and spectral bandwidth for the exposure light, and engineered absorption properties of the photosensitive materials. We also describe approaches in which soft nanoimprinting processes introduce surface relief directly into the photosensitive materials, to create phase modulating or other structures that can be used alone or together with PnP masks to yield additional classes of 3D structures.

3.1. Periodic Structures by One-Photon PnP. The use of one-photon processes for exposure represents one form of PnP. Here, each incident photon has sufficient energy to initiate the chemical processes that lead to solid 3D structures in the photosensitive material. Figure 4 shows some representative structures formed by one-photon PnP in SU-8 with various phase masks and exposure wavelengths at 355 and 514 nm from the frequency tripled Nd:YAG laser and Ar-ion laser, respectively, and with 365 nm light from a mercury lamp.³⁵ These examples range from interconnected, structured elliptical elements to interleaved nanochannels. In all cases, the phase mask defines the dominant spatial Fourier component in the in-plane direction. The Talbot and related effects determine the variations of the structures through the depth of the material. In general, as the periodicity of the features of relief on the masks decreases relative to the wavelength of the exposure light, the 3D structures exhibit fewer spatial Fourier components, consistent with both

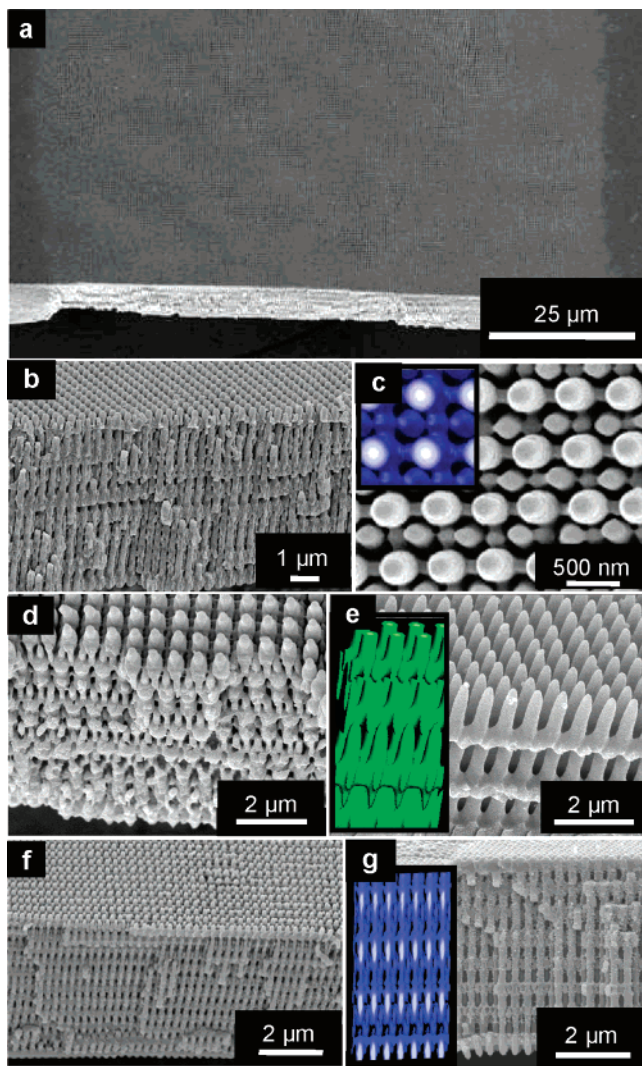


Figure 4. Scanning electron micrographs of representative 3D nanostructures formed by one-photon PnP. (a) Large view of a 3D structure formed with 355 nm light (tripled Nd:YAG) and a phase mask that consists of square array of posts ($d = 375$ nm, $RD = 420$ nm, $p = 566$ nm). (b) and (c) side and top views of the structure in (a), respectively. The inset in (c) shows modeling results. (d) and (e) 3D structures generated with a single phase mask ($d = 570$ nm, $RD = 420$ nm, $p = 1140$ nm) using 355 and 514 nm (Ar ion) laser light, respectively. The inset in (e) provides modeling results. (f) and (g) angled and side views of structures generated using the filtered output of a mercury lamp. The phase mask in (f) and (g) is the same as that used in (a). The inset in (g) provides modeling results.

the Abbe and Talbot images of the optics. As an example of this effect, parts d and e of Figure 4 show structures formed with a single phase mask at exposure wavelengths of 355 and 514 nm, respectively. The structures have similar periodicities in the plane, but longer out-of-plane periods and fewer spatial Fourier components for 514 nm light compared to 355 nm. The exposures can be implemented also with incoherent light from UV lamps, due to the relaxed requirements on spatial and temporal coherence of the exposure light associated with the proximity mode geometry. This feature suggests a capability for scaling to large areas, allowing for the potential use of a large base of installed semiconductor wafer contact lithography tools, and extensions into plate exposure systems used for flat panel displays and for printing plates used for large printing presses. In the examples of Figure 4f,g, the exposure light was derived from a mercury lamp, geometrically collimated with a tube and spectrally filtered with an interference filter centered

at 365 nm. The structures fabricated in this fashion have geometries similar to those formed with the 355 nm laser light. In these and all other cases, modeling in which computed intensity distributions are converted to predicted 3D structure geometries through the application of a cutoff filter to simulate the exposure and development processes, agrees well with the observed shapes. Other mask geometries, such as hexagonal arrays of posts, parallel lines, aperiodic array of dots, and multilevel phase masks can also generate useful structures.^{35–41} This design flexibility represents an important feature of PnP.

3.2. Periodic Structures by Two-Photon PnP. The proximity geometry of PnP also enables the use of short pulsed lasers for the exposures.^{38,41} Such lasers can offer sufficiently high powers that two-photon interactions in commercially available photosensitive materials such as SU8 can be used in patterning. A two-photon process involves the simultaneous absorption of photons that have energies equal to or somewhat more than one-half of that needed to activate the photosensitizer.^{11,79} For SU8, the minimum peak power required for practical use of such a process is ~ 1 TW/cm² at wavelengths of ~ 800 nm. The output of a regeneratively amplified Ti:sapphire laser (Spectra-Physics, Spitfire Pro) provides a convenient light source for this purpose. The wavelength in this case is ~ 800 nm; required peak powers can be obtained with beam diameters of > 1 mm, pulse durations of ~ 140 fs, and pulse energies of ~ 2 mJ. For distances less than ~ 10 μ m from the surface of a mask, the effects of spectral or temporal walkoff associated with diffraction can, to a first approximation, be neglected.^{38,41} The ease with which short pulses can be used in PnP contrasts with the technical difficulties associated with matching path lengths to achieve temporal overlap of multiple beams in holography approaches.^{80,81} The ability to perform two-photon PnP patterning in a single step provides advantages over the generally slow, serial operation of traditional two-photon writing approaches.^{11,32} Compared to one-photon PnP, the two-photon process provides enhanced contrast ratios due to the quadratic dependence of the exposure on the intensity. In addition, the comparatively long wavelengths used in the two-photon process yield fewer numbers of spatial Fourier components in the 3D structures than the corresponding one-photon process. As a result, two-photon PnP provides access to lattice geometries that are not easily achieved with one-photon interactions, such as symmetrically simple structures that can be useful for photonic band gap materials and other applications.^{38,41} Higher order interactions (e.g., three-photon processes) should also be possible, with suitably designed materials.

Figure 5 illustrates some results from two-photon PnP using phase masks with square and hexagonal geometries at different periodicities and relief depths.³⁸ For the structure of Figure 5a, the mask consisted of a square array of circular posts ($d = 570$ nm, $RD = 510$ nm, and $p = 710$ nm). The periodicity of the phase mask, in this case, is less than the wavelength of the light used for the two-photon exposure (~ 800 nm); no diffracted beams appear when 800 nm light passes through the mask in air. Contact with the relatively-high-index SU-8 material, however, results in 9 diffracted beams that generate the 3D intensity distributions corresponding to the structures of Figure 5a. In this regime of subwavelength mask layouts, the state of polarization of the exposure light can have pronounced effects on the geometries.³⁸ In particular, directionality in the 3D intensity distributions can be produced throughout the thickness of photopolymer by using linearly polarized light, as shown in Figure 5d. Circular polarization leads to isotropic structures, as shown in Figure 5e. Polarization can, in this way, provide an additional parameter for controlling the geometries.

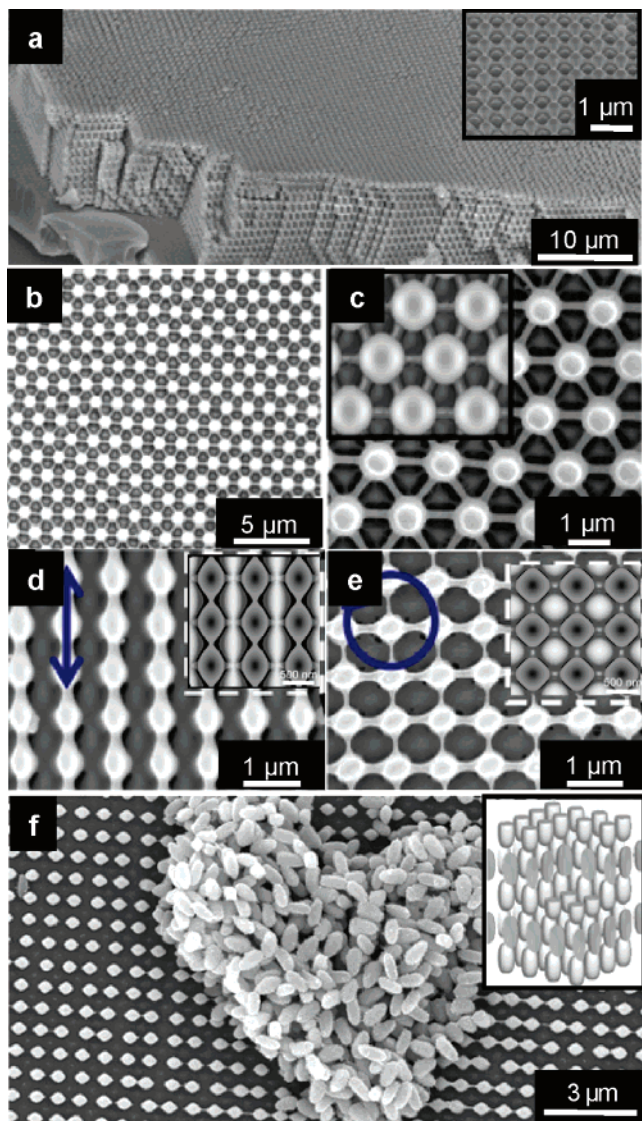


Figure 5. Scanning electron micrographs (SEMs) of representative 3D nanostructures formed by two-photon PnP. (a) Large area angled and top (inset) views of a structure generated using a phase mask with relief consisting of square array of posts ($d = 570$ nm, $h = 510$ nm, $p = 710$ nm) and the regeneratively amplified output of a Ti:sapphire laser operating at 800 nm. (b) and (c) SEM top views of structures made with this same laser using a phase mask with relief consisting of a triangular array of posts ($d = 1120$ nm, $h = 420$ nm, $p = 1500$ nm). The inset in (c) shows modeling results. (d) and (e) top view SEMs of structures generated using linear (along the [0, 1] direction of the mask) and circular polarized light with the mask used for the structure in (a), respectively. The insets show modeling results. (f) SEM of ellipsoidal particles and modeling (inset) generated using the phase mask in (a).

The exposure contrast provided by the two-photon interaction allows the formation of not only 3D structures but also collections of individual structures. In particular, by suitable control of the exposure and development conditions, PnP can form large numbers of colloidal particles, wires and other objects with classes of shapes that would be difficult to generate in other ways.³⁸ Figure 5f shows examples of ellipsoidal particles formed with the mask used for the structure of Figure 5a. These and other types of colloidal particles can be used for fundamental studies of assembly⁸² as well as applications in photonics and chemical sensing.^{4,83}

3.3. Density Graded Structures. In addition to polarization, wavelength and interaction processes (i.e., one or two photon,

or more generally multiphoton), the angular and spectral bandwidth of the exposure light can influence the structural geometries in a controllable manner. For example, these parameters, as well as the absorption strength of the photosensitive material at the exposure wavelength, can be used to control variations in the average pore sizes in the 3D structures through their thicknesses, in a monotonic or nonmonotonic fashion. Such layouts provide classes of density gradient structures (DGS) that are of interest for chemical/drug release, high-energy density science targets, impact resistance materials, and others.^{39,40,58,84} DGS can be achieved via PnP through control of exposure angles,³⁹ exposure bandwidth,³⁹ or absorption in the photosensitive material.⁴⁰ The first strategy involves, for example, sequential exposures at angles of 0° (i.e., normal to the surface of the mask), $-\theta$ and $+\theta$ or exposures with diverging/converging beams. The rate of change in the degree of porosity (i.e., effective density) through the thickness of the 3D structures increases with angular bandwidth. For sequential exposures, this change is periodic with depth, yielding nonmonotonic variations in porosity with thicknesses.³⁹ Purely monotonic DGS, in thick geometries (i.e., up to ~ 100 μm), can be created by introducing controlled levels of absorption in the photosensitive polymer through the addition of dyes.⁴⁰ Here, absorption causes the average exposure dose to decrease as the light propagates through the material, leading to associated increases in the level of porosity in the resulting structures. Figure 6 shows an example of a thick DGS formed in this way, using a backside exposure geometry in which the phase mask contacts a transparent substrate that supports a film of SU8 on the opposite side.⁴⁰ Figure 6c shows an electron micrograph indicating the variation in effective density of a representative DGS, where the density ranges from 19% to 100% of full density over a thickness of 60 μm distance. The magnitude of the density gradient can be adjusted by controlling the strength of absorption in the SU8.

3.4. Aperiodic Structures. The examples discussed thus far use phase masks with periodic arrays of posts, holes, and lines and other structures. PnP can, however, be performed with much more complex mask designs. In particular, aperiodic 3D structures can be formed by PnP with aperiodic mask layouts.³⁵ Figure 7 illustrates an example of a mask that consists of a square array of cylindrical posts, with an isolated defect in the form of a missing post.³⁵ This missing post causes a local variation in intensity, beginning in the near field but persisting and broadening as a function of distance away from the mask. Parts a and b of Figure 7 show top-views of the mask and the 3D structure, respectively. Parts c and d of Figure 7 show confocal images of the structure as a function of depth, at a plane some distance away from the defect and approximate calculations performed with the Abbe approach.³⁵ Further study of the effects of such defects and, more generally, implementation of complex mask designs derived using inverse computational methods to achieve user-specified 3D geometries, are topics of current research.

3.5. Structures Formed with Quasicrystal Phase Masks. An advanced type of phase mask that lacks long-range periodicity consists of relief features in quasicrystalline layouts. One promise of such masks in PnP is that they might enable the formation of full 3D quasicrystals or related structures, of the type that might be useful in photonic band gap (PBG) applications.^{57,85,86} 3D quasicrystals are of interest because they can possess an approximately spherical Brillouin zone,^{88–90} leading to the possibility of complete PBGs with smaller refractive index contrast compared to those required in conventional periodic layouts. For example, a PBG in a 2D quasicrystal lattice is

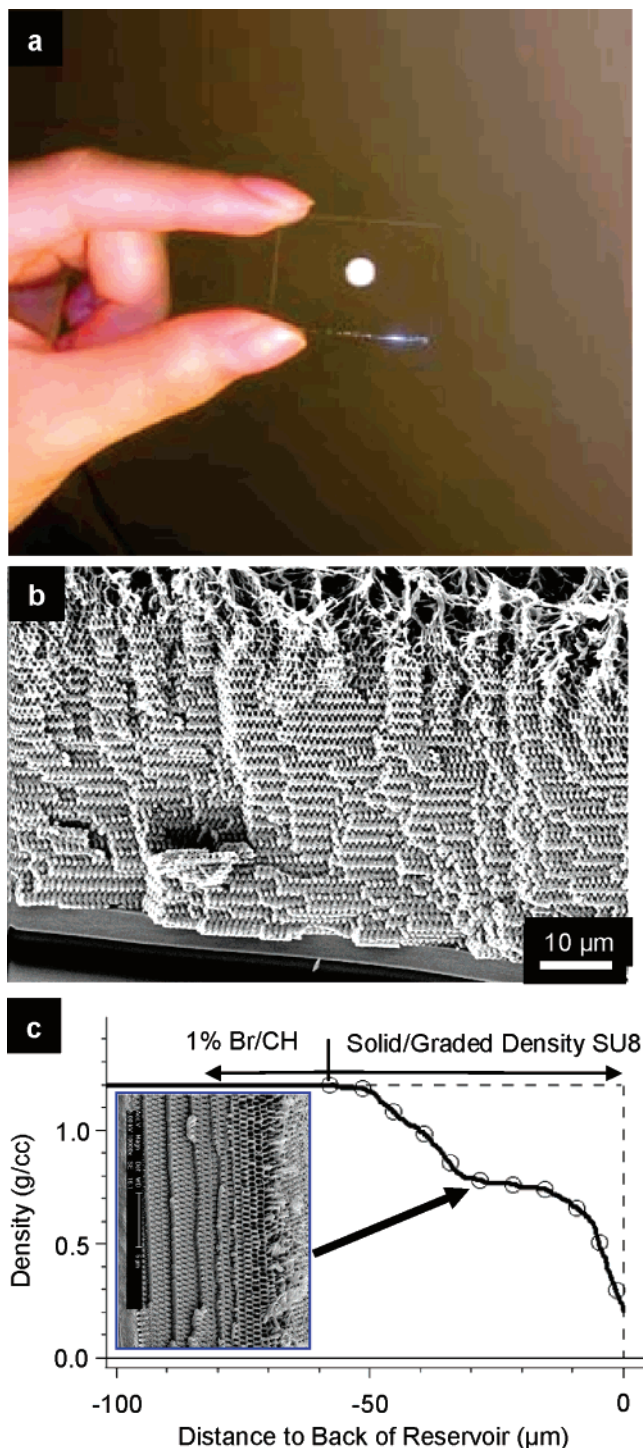


Figure 6. Density gradient structure (DGS) generated by one-photon PnP using an a-PFPE phase mask with relief consisting of a hexagonal array of cylindrical posts ($d = 460$ nm; $RD = 420$ nm; $p = 600$ nm). (a) Optical image of a DGS film on a glass substrate. (b) Scanning electron micrograph of a cross section of this sample. (c) Plot of relative density with position through the thickness of the sample from X-ray radiographs.

possible with an index contrast of 1.45, compared to ~ 2.5 for a hexagonal layout.⁸⁹ The fabrication of 3D quasicrystals with dimensions in a range suitable for operation at visible or near-infrared wavelengths is, however, extremely challenging. Recent work demonstrates the ability to make multilayered 2D quasicrystals by interfering 10 laser beams.⁸⁷ True 3D quasicrystals with 5-fold symmetry have been generated by two-photon direct-write,⁸⁵ but the fabrication process can be slow. As a result,

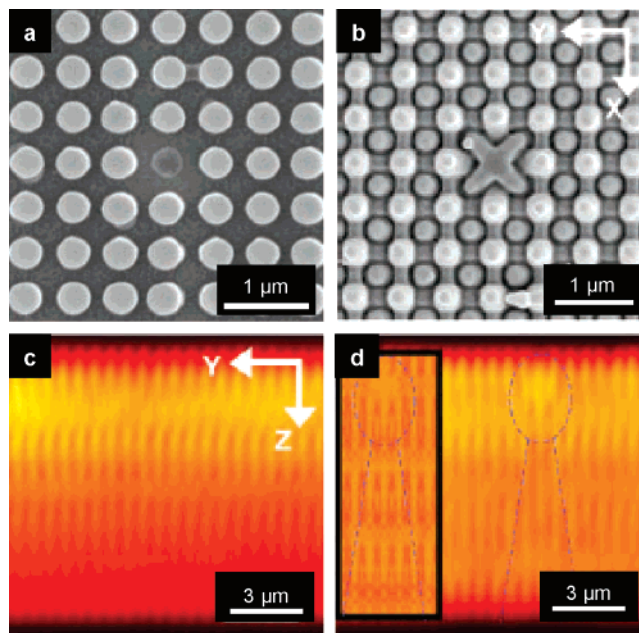


Figure 7. (a) and (b) scanning electron micrographs of the top of a phase mask with relief consisting of a square array of posts ($d = 375$ nm, $RD = 420$ nm, and $p = 566$ nm) with a isolated missing dot and corresponding 3D structure formed by one-photon PnP, respectively. (c) Confocal micrograph of the $x-z$ plane of the structure imaged at a position along y that is far from the missing post (i.e., defect structure). (d) Similar image collected at the location of the defect. The inset shows modeling results. The dotted line highlights certain features.

there is interest in exploring PnP with quasicrystal phase masks for these and other applications. Independent work by another group recently demonstrated the ability to use the PnP method with quasicrystal masks formed by casting and curing PDMS against masters that consist of photoresist patterned by multiple, crossed exposures in line grating geometries.⁸⁶

Figure 8 presents some results of PnP with masks that have Penrose quasicrystal layouts consisting of holes with diameters of 400 nm and average hole to hole spacings of 800 nm. The pattern has a global 10-fold rotational symmetry that generates hundreds of diffracted beams, as shown in Figure 8b. These beams overlap and interfere to form a complex distribution of intensity near the surface of the mask, as illustrated in the NSOM images of Figure 8e–g. Exposing the SU8 using a “maskless” two-photon procedure described in the following section, followed by developing leads to 3D structures like the one shown in Figure 8h. A two-photon process, similar to that described in section 3.2 was used in this case to produce structures with high symmetry and high stability. Preliminary measurements indicate an absence of a simple unit cell in these systems, reminiscent of quasicrystal geometries. These results illustrate the feasibility of generating well-defined 3D structures with Penrose quasicrystal masks. Additional study is needed to define the optics associated with the fabrication process, as well as the geometries of the 3D structures and their optical properties.

3.6. Hierarchical and Other Structures by Molding and PnP. Molding and soft nanoimprint lithography, performed with phase masks or similar elements as molds, can be combined with PnP concepts to yield structures with hierarchical and other structure geometries that are inaccessible with PnP alone. A simple case corresponds to the use of embossed features of relief on the photosensitive material as the phase mask for PnP.⁴¹ We refer to this process as “maskless” PnP because it does not require, although it can exploit, a separate phase mask during

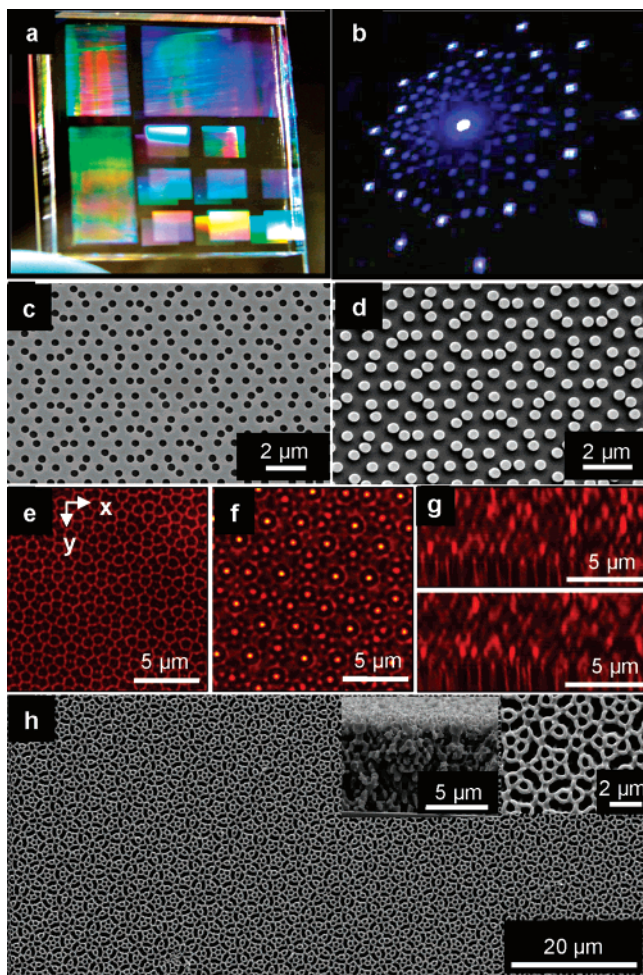


Figure 8. Images associated with one and two-photon PnP using phase masks with Penrose quasicrystal layouts. (a) Image of a phase mask with different regions that correspond to quasicrystals with different characteristic sizes and periods. (b) Far field diffraction pattern generated by passing 355 nm light through a region of this mask that has a Penrose quasicrystal layout with $d = 400$ nm and average $p = 800$ nm. This mask produces hundreds of diffracted beams. (c) and (d) scanning electron micrographs of a representative region of a Penrose quasicrystal “master” and of a corresponding phase mask, respectively. (e) and (f) near field scanning optical microscope (NSOM) images collected at the surface of a Penrose quasicrystal phase mask in (d) and at distances from the surface of the mask (i.e., z) of 0 and 2.4 nm, respectively. (g) and (h) NSOM images of the x - z plane at $z = 0$ μm and $z = 1.50$ μm , respectively. (i) Top view SEM of 3D structures generated by two-photon PnP with a Penrose quasicrystal phase mask. In this case, the surface of the photosensitive material was molded with the mask, and the exposure was performed in a “maskless” mode where the molded features of relief phase modulate the exposure light. The insets in (h) show cross-sectional (left) and top view (right) SEMs.

the exposure step. Maskless PnP can facilitate large area processing and improve the optical contrast by eliminating mask/film reflections, and it also reduces the amplitude of relief required to achieve high levels of phase modulation, due to the relatively high index of refraction of a photosensitive material such as SU8 compared to the PDMS or PFPE. Figure 9 provides an overview of the process and an example of a 3D structure formed using molded relief consisting of square arrays of holes ($d = 375$ nm, $\text{RD} = 420$ nm, and $p = 566$ nm). This embossed mask yields a phase modulation of $\sim 0.6\pi$ for transmitted light. Achieving this level of modulation with a PDMS mask would require relief depths of 690 nm, which are difficult to achieve with posts that have diameters of 375 nm, using existing PDMS

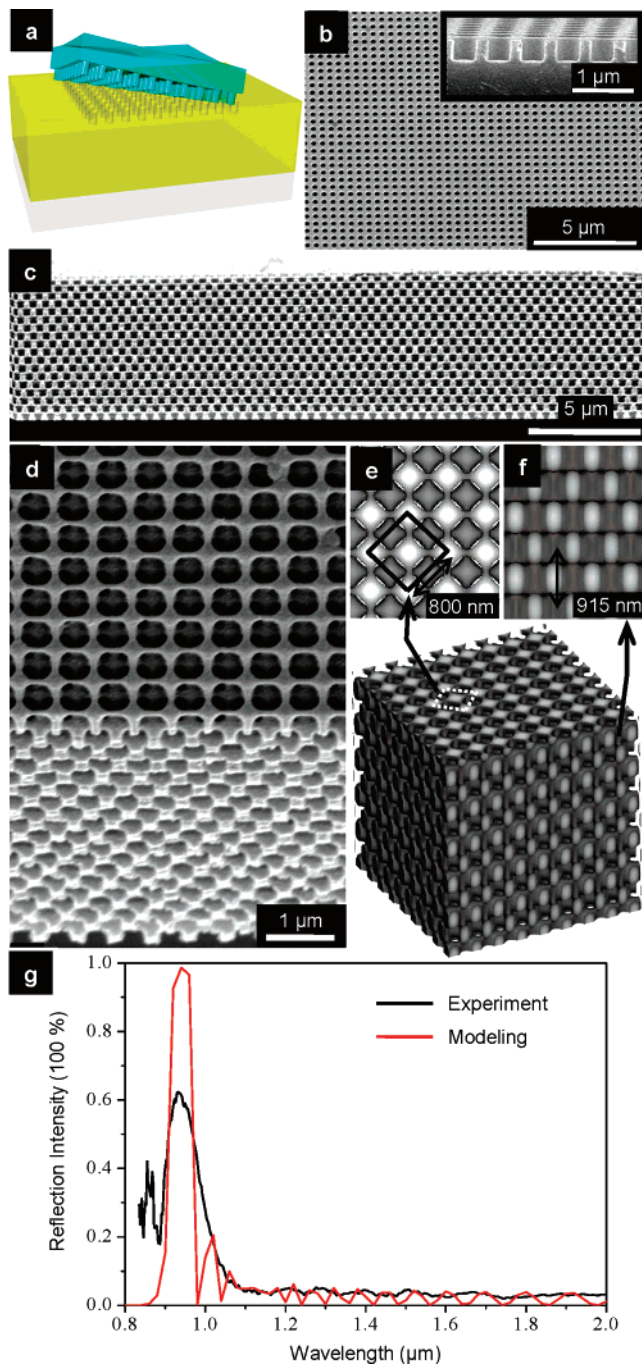


Figure 9. Schematic illustrations and scanning electron micrographs of 3D nanostructures formed by two-photon PnP using exposure through a layer of the photopolymer SU-8 molded with a phase mask consisting of a square array of posts ($d = 375$ nm, $\text{RD} = 420$ nm, and $p = 566$ nm). (a) Schematic illustration of the molding process. (b) Top and cross sectional (inset) SEMs of the molded SU8. (c) and (d) cross section and angled view SEMs, respectively, of the resulting 3D structure. (e) and (f) intensity distributions along the (001) plane and the (110) plane, respectively, of the full computation as rendered in 3D through application of a cutoff filter, shown below. (g) Experimental and theoretical reflection spectra for these structures.

or PFPE formulations. The contrast improves by 50 times compared to the case of a mask based exposure and the same phase shift.

A combination of coarse (several microns) and fine molded features can be used with separate PnP masks to enable structures that are impossible to produce using conventional PnP alone. Figure 10 provides the fabrication scheme for molded rib waveguides with internal 3D nanostructures, of the sort that

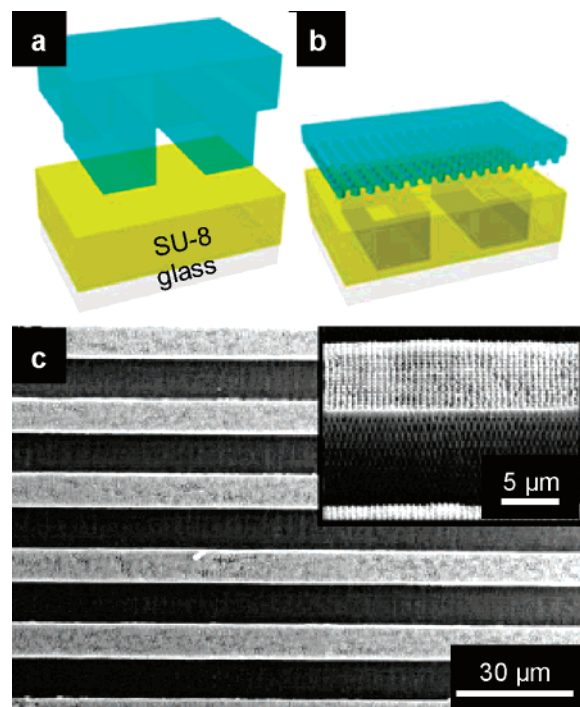


Figure 10. Schematic illustrations and scanning electron micrographs (SEMs) of 3D structures formed by molding coarse ($\sim 10 \mu\text{m}$ widths and depths) features into a layer of SU-8 (a), and then performing PnP on the molded structure (b). (c) Top and angled view (inset) SEMs of the resulting 3D structures. The phase mask consists of a square array of posts ($d = 375 \text{ nm}$, $\text{RD} = 420 \text{ nm}$, and $p = 566 \text{ nm}$).

might be useful for applications in microfluidics or optical waveguides. The use of fine molded structures with phase masks can create multiple levels of phase modulation to achieve, for example, woodpile-type 3D structures. Figure 11 shows such a process. The 3D structure generated by this type of effective multilevel phase mask can be seen in Figure 11c,d. In all cases, the geometries of the structures, in regions away from the molded surface regions, can be reproduced accurately by modeling.

4. Applications

The wide range of 3D structures that can be generated by PnP, as illustrated in the previous sections, create many application possibilities. The following provides some examples that we have explored in recent work.

4.1. Filters and Mixers for Microfluidics. Microfluidic systems benefit from filters, separation membranes, passive and active mixers, and other devices that can be integrated directly into tens of micron sized channels. In many cases, these elements can be achieved with the sorts of 3D nanostructures that can be produced easily by PnP.^{35,37} Mixers represent one example. There are two classes of such devices: (i) active systems, which use external forces generated by micron scale stir bars,⁹⁰ peristaltic pumps,⁹¹ and others^{92,93} and (ii) passive systems, which use geometrical features, such as fluted sidewalls,⁹⁴ meanders,^{1,2,93,95} and related structures.⁹⁴ Active mixers provide high efficiencies at small sizes, but they are typically complex and difficult to integrate. Passive mixers do not require power, but they provide relatively low efficiencies and often require challenging fabrication steps (e.g., multilevel 3D structures). Certain classes of passive devices use multiple substream flow paths to provide chaotic mixing and laminating flows that can reduce the distances for diffusive mixing.^{93,94,96} The required

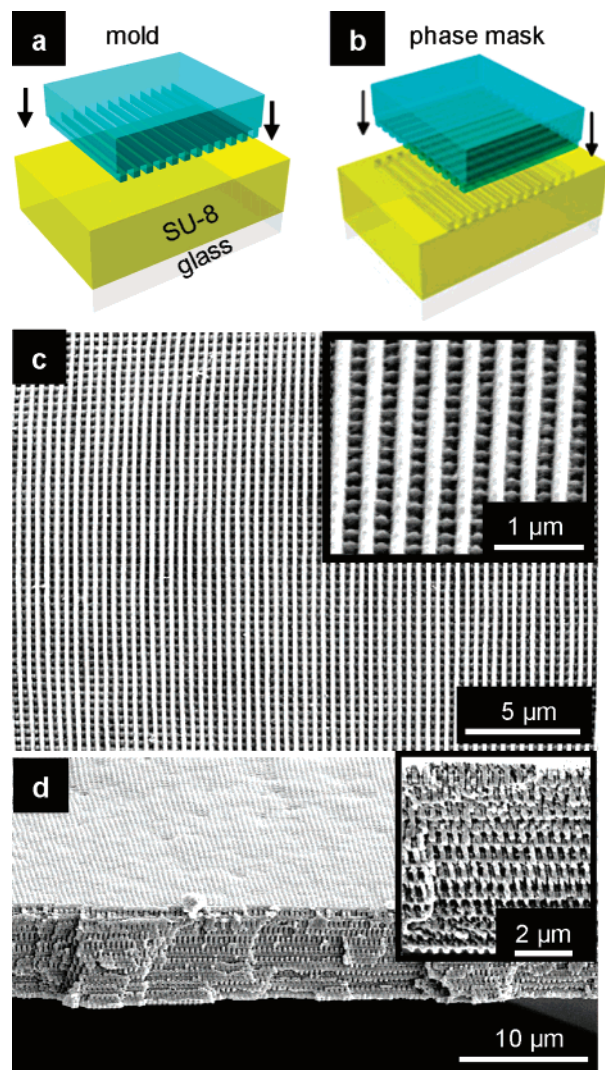


Figure 11. Schematic illustrations and scanning electron micrographs (SEMs) of 3D structures formed by molding fine features (equally spaced lines and spaces with $\text{RD} = 220 \text{ nm}$ and $p = 400 \text{ nm}$) into a layer of SU-8 (a) and then performing PnP on the molded structure with the same element used for the molding but with a ninety degree rotation. (c) and (d) show low- and high-magnification top view and cross sectional SEMs of the resulting 3D structures.

sizes for these substream flow channels are often substantially less than $1 \mu\text{m}$, making integration in the form of large scale 3D arrays difficult for conventional fabrication techniques. This type of patterning task, on the other hand, is relatively simple using the PnP approach. Hundreds or even thousands of substream flow paths with dimensions down to the 50 nm range can be generated directly in microfluidic channels in a single exposure step. Figure 12 shows an example of such a passive mixer built into a serpentine microfluidic channel. The images indicate good structure uniformity and robust operation with widths of flow paths between 50 and 300 nm . The resulting passive device exhibits high mixing efficiencies even under small Reynolds numbers, likely due to multiple laminating flows forced by the 3D structure layout.³⁷ Similar structures can be used as microfluidic filters and separation membranes.³⁵ In a simple example, the submicron channels generated by PnP serve as filters for separating submicrometer particles from fluid flows.³⁵ Figure 12d provides an image.

4.2. Density Gradient Structures for High-Energy Density Science Targets and Chemical Release. Density gradient

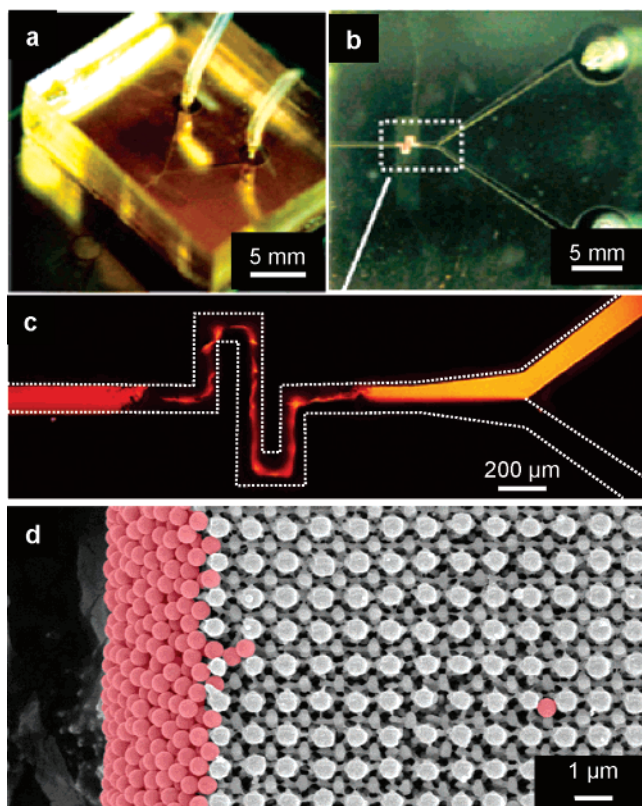


Figure 12. (a) and (b) image and micrographs, respectively, of a microfluidic device that contains an integrated 3D nanostructure formed by one-photon PnP. (c) Confocal micrograph of a microfluidic mixer that consists of a 3D nanostructure embedded in a serpentine channel, collected at a flow velocity (right to left) of 6.67 mm/s. The red in these images corresponds to fluorescence recorded from Rhodamine dye in water using laser excitation at 514 nm (Ar ion). The uniform red color at the output (left) indicates good mixing of the initially unmixed, laminar streams at the input (right). (d) Scanning electron micrograph of a 3D nanostructure filter built into the channel of a microfluidic system (flow from left to right). The colorized red beads are filtered at the edge of the structure.

structures (DGS) have many potential applications, as mentioned previously. In one example, time dependent release of chemicals imbedded into DGS materials can be controlled by tuning the size and spatial gradients in the porosity. Experimental results show that for the case of riboflavin filled into a DGS formed by absorption controlled PnP, the chemical release kinetics can be modified.⁴⁰ In a different application, thick DGS serve as encapsulating layers in reservoir targets for high-energy density science.⁵⁷ In this application, appropriately designed DGS can shape the pressure profiles formed during shockless compression by slowing the transfer of momentum into the target. The goal of using DGS in shockless compression is to increase the rise time to reach certain peak stress. Figure 13 shows a time history of the ramp pressure profile resulting from a DGS (inset) designed for this purpose, whose variation in density appears in Figure 6c. The data indicate a 30% increase in time required to achieve similar levels of stress in the DGS compared to the solid structure.⁵⁷ This increase in rise time makes it possible to achieve higher peak stress without shocking the sample in the DGS system.⁵⁷

4.3. Photonic Band Gap Materials. The requirements for 3D PBG materials are potentially well matched to the capabilities of PnP. PBG materials involve periodic variations in refractive index that create a range of frequencies, known as a photonic bandgap, in which photons cannot propagate in any

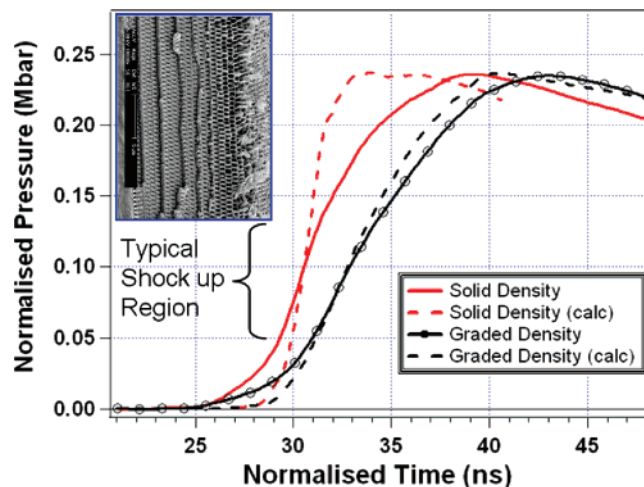


Figure 13. Pressure profile as a function of time with and without a density gradient produced by PnP in a layer of SU-8. The dashed lines are calculated pressure profiles. The pressure and time axes have been normalized.

direction within the material^{97,98} This behavior can be exploited for many applications such as sharp bend waveguides,⁹⁹ channel-drop filters,¹⁰⁰ wide-angle splitter,¹⁰¹ and others.¹⁰² Although theory predicts the existence of several 3D geometries that should result in complete PBGs,^{97,98,103,104} the fabrication can be prohibitively challenging for realistic applications. Approaches ranging from conventional photolithography,^{105,106} colloidal self-assembly,^{7,18,107,108} to laser or direct ink writing,^{7,11,109} and holographic interference lithography^{26–29,110} have been explored. Compared to these techniques, PnP might provide advantages in terms of large area processing, design flexibility and simple, low-cost operation. With maskless PnP, it is possible to fabricate 3D structures with symmetries close to face center cubic (FCC), similar to those in Figure 9. These structures exhibit high normal incidence reflection ($\sim 60\%$), as measured by Fourier transform infrared spectroscopy (FTIR) (Bruker Optics Inc., model Hyperion 1000). Figure 9f shows measurements and calculations.⁴¹ Although there is good agreement in the wavelength position of the reflection, the magnitude in the measured case is somewhat lower than that of the theoretical prediction.⁴¹ The discrepancy can be explained by minor structural disorder and shrinkage upon developing. Improved photosensitive materials, together with alternative PnP approaches that use masks with multilevel or quasicrystalline layouts, represent subjects of current work.

5. Conclusion

In conclusion, proximity field nanopatterning, or PnP, represents a simple optical method that provides experimentally convenient routes to wide ranging classes of 3D nanostructures, in large area coverages (several square centimeters and larger) and in thick geometries (up to $\sim 100 \mu\text{m}$). Talbot effect optics, elastomeric phase modulating masks, and thick transparent photosensitive materials are keys to the approach. This Feature Article summarizes these aspects, as well as certain patterning capabilities enabled by engineered mask designs, exposure sources and optics, and materials. Several application examples in microfluidics, chemical release, high-energy density science, colloidal particle fabrication and photonics were described. Future opportunities exist in these and other applications, as well as in further development of the patterning approach. As an example of the latter, inverse computational algorithms

should allow masks to be designed to achieve desired structure outcomes. These and other aspects appear to be promising directions for research.

Acknowledgment. D.J.S., S.J., H.L., M.H., D.G.C., and J.A.R. contributed equally to this work. This work is supported by DOE-LLNL through grant B529271, DOE through grant No. DEFG02-91ER45439, and NSF through grant DMI 03-55532 and DMR-0415187. The facilities included the Frederick Seitz Materials Research Laboratory, University of Illinois, which is partially supported by the U.S. Department of Energy under grant DEFG02-91-ER45439, and Sandia National Laboratories, a multiprogram laboratory operated by Sandia Corp., a Lockheed Martin Co., for the U.S. Department of Energy's National Nuclear Security Administration under contract DE-AC04-94AL85000. Use of the Center for Nanoscale Materials was supported by the U.S. Department of Energy, Office of Science, Office of Basic Energy Sciences, under Contract No. W-31-109-Eng-38.

References and Notes

- Moorthy, J.; Mensing, G. A.; Kim, D.; Mohanty, S.; Eddington, D. T.; Tepp, W. H.; Johnson, E. A.; Beebe, D. J. *Electrophoresis* **2004**, *25*, 1705.
- Vijayendran, R. A.; Motsegood, K. M.; Beebe, D. J.; Leckband, D. E. *Langmuir* **2003**, *19*, 1824.
- Pregibon, D. C.; Toner, M.; Doyle, P. S. *Langmuir* **2006**, *22*, 5122.
- Holtz, J. H.; Asher, S. A. *Nature* **1997**, *389*, 829.
- Grier, D. G. *Nature* **2003**, *424*, 810.
- Christodoulides, D. N.; Lederer, F.; Silberberg, Y. *Nature* **2003**, *424*, 817.
- Braun, P. V.; Rinne, S. A.; Garcia-Santamaria, F. *Adv. Mater.* **2006**, *18*, 2665.
- Long, J. W.; Dunn, B.; Rolison, D. R.; White, H. S. *Chem. Rev.* **2004**, *104*, 4463.
- Holland, B. T.; Blanford, C.; Stein, A. *Science* **1998**, *281*, 538.
- Chai, G. S.; Shin, I. S.; Yu, J. S. *Adv. Mater.* **2004**, *16*, 2057.
- Cumpston, B. H.; Ananthavel, S. P.; Barlow, S.; Dyer, D. L.; Ehrlich, J. E.; Erskine, L. L.; Heikal, A.; Kuebler, S. M.; Lee, I. Y. S.; McCord-Maughon, D.; Qin, J.; Rockel, H.; Rumi, M.; Wu, X.-L.; Marder, S. R.; Perry, J. W. *Nature* **1999**, *398*, 51.
- Parthenopoulos, D. A.; Rentzepis, P. M. *Science* **1989**, *245*, 843.
- Gates, B. D.; Xu, Q. B.; Stewart, M.; Ryan, D.; Willson, C. G.; Whitesides, G. M. *Chem. Rev.* **2005**, *105*, 1171.
- Wallraff, G. M.; Hinsberg, W. D. *Chem. Rev.* **1999**, *99*, 1801.
- Dinsmore, A. D.; Hsu, M. F.; Nikolaides, M. G.; Marquez, M.; Bausch, A. R.; Weitz, D. A. *Science* **2002**, *298*, 1006.
- Jiang, P.; Cizeron, J.; Bertone, J. F.; Colvin, V. L. *J. Am. Chem. Soc.* **1999**, *121*, 7957.
- Velev, O. D.; Jede, T. A.; Lobo, R. F.; Lenhoff, A. M. *Nature* **1997**, *389*, 447.
- Vlasov, Y. A.; Bo, X. Z.; Sturm, J. C.; Norris, D. J. *Nature* **2001**, *414*, 289.
- Bates, F. S. *Science* **1991**, *251*, 898.
- Boltau, M.; Walheim, S.; Mlynek, J.; Krausch, G.; Steiner, U. *Nature* **1998**, *391*, 877.
- Kim, S. O.; Solak, H. H.; Stoykovich, M. P.; Ferrier, N. J.; de Pablo, J. J.; Nealey, P. F. *Nature* **2003**, *424*, 411.
- Furieux, R. C.; Rigby, W. R.; Davidson, A. P. *Nature* **1989**, *337*, 147.
- Trau, M.; Yao, N.; Kim, E.; Xia, Y.; Whitesides, G. M.; Aksay, I. A. *Nature* **1997**, *390*, 674.
- Jacobs, H. O.; Tao, A. R.; Schwartz, A.; Gracias, D. H.; Whitesides, G. M. *Science* **2002**, *296*, 323.
- Yeh, H. J. J.; Smith, J. S. *IEEE Photon. Technol. Lett.* **1994**, *6*, 706.
- Campbell, M.; Sharp, D. N.; Harrison, M. T.; Denning, R. G.; Turberfield, A. J. *Nature* **2000**, *404*, 53.
- Divliansky, I.; Mayer, T. S.; Holliday, K. S.; Crespi, V. H. *Appl. Phys. Lett.* **2003**, *82*, 1667.
- Lillal, C. K.; Maldovan, M.; Thomas, E. L.; Chen, G.; Han, Y.-J.; Yang, S. *Appl. Phys. Lett.* **2004**, *84*, 5434.
- Yang, S.; Megens, M.; Aizenberg, J.; Wiltzius, P.; Chaikin, P. M.; Russel, W. B. *Chem. Mater.* **2002**, *14*, 2831.
- Matthias, S.; Muller, F.; Gosele, U. *J. Appl. Phys.* **2005**, *98*, 023524.
- Matthias, S.; Mueller, F. *Nature* **2003**, *424*, 53.
- Kawata, S.; Sun, H.-B.; Tanaka, T.; Takada, K. *Nature* **2001**, *412*, 697.
- Galajda, P.; Ormos, P. *Appl. Phys. Lett.* **2001**, *78*, 249.
- Gratton, G. M.; Xu, M. J.; Lewis, J. A. *Nature* **2004**, *428*, 386.
- Jeon, S.; Park, J.-U.; Cirelli, R.; Yang, S.; Heitzman, C. E.; Braun, P. V.; Kenis, P. J. A.; Rogers, J. A. *Proc. Natl. Acad. Sci. U.S.A.* **2004**, *101*, 12428.
- Jeon, S.; Menard, E.; Park, J. U.; Maria, J.; Meitl, M.; Zaumseil, J.; Rogers, J. A. *Adv. Mater.* **2004**, *16*, 1369.
- Jeon, S.; Malyarchuk, V.; White, J. O.; Rogers, J. A. *Nano Lett.* **2005**, *5*, 1351.
- Jeon, S.; Malyarchuk, V.; Rogers, J. A.; Wiederrecht, G. P. *Optics Express* **2006**, *14*, 2300.
- Jeon, S.; Nam, Y. S.; Shir, D.; Rogers, J. A. *Appl. Phys. Lett.* **2006**, *89*, 253101.
- Jeon, S.; Shir, D.; Nam, Y.; Nidetz, R.; Highland, M.; Cahill, D.; Rogers, J.; Su, M.; Ihab, E.; Christodoulou, C.; Bogart, G. *Appl. Opt.*, submitted for publication.
- Jeon, S.; Shir, D.; Nam, Y. S.; Rogers, J. A. *Optics Express* **2007**, *15*, 6354-62.
- Zhou, W.; Huang, Y.; Menard, E.; Aluru, N. R.; Rogers, J. A.; Alleyne, A. G. *Appl. Phys. Lett.* **2005**, *87*, 251925.
- Huang, Y. G. Y.; Zhou, W. X.; Hsia, K. J.; Menard, E.; Park, J. U.; Rogers, J. A.; Alleyne, A. G. *Langmuir* **2005**, *21*, 8058.
- Hsia, K. J.; Huang, Y.; Menard, E.; Park, J. U.; Zhou, W.; Rogers, J.; Fulton, J. M. *Appl. Phys. Lett.* **2005**, *86*, 154106.
- Xia, Y.; Whitesides, G. M. *Angew. Chem., Int. Ed. Engl.* **1998**, *37*, 550.
- Xia, Y.; Rogers, J. A.; Paul, K. E.; Whitesides, G. M. *Chem. Rev.* **1999**, *99*, 1823.
- Schmid, H.; Michel, B. *Macromolecules* **2000**, *33*, 3042-3049.
- Odom, T. W.; Love, J. C.; Wolfe, D. B.; Paul, K. E.; Whitesides, G. M. *Langmuir* **2002**, *18*, 5314.
- Rolland, J. P.; Hagberg, E. C.; Denison, G. M.; Cater, K. R.; DeSimone, J. M. *Angew. Chem., Int. Ed.* **2004**, *43*, 5796.
- Truong, T. T.; Lin, R.; Jeon, S.; Lee, H. H.; Maria, J.; Gaur, A.; Hua, F.; Meinel, I.; Rogers, J. A. *Langmuir* **2007**, *23*, 2898.
- Hua, F.; Gaur, A.; Sun, Y.; Word, M.; Niu, J.; Adesida, I.; Shim, M.; Shim, A.; Rogers, J. A. *IEEE Trans. Nanotechnol.* **2006**, *5*, 301.
- Hua, F.; Sun, Y.; Gaur, A.; Meitl, M. A.; Bilhaut, L.; Rotkina, L.; Wang, J.; Geil, P.; Shim, M.; Rogers, J. A.; Shim, A. *Nano Lett.* **2004**, *4*, 2467.
- Gates, B. D.; Whitesides, G. M. *J. Am. Chem. Soc.* **2003**, *125*, 14986.
- Rogers, J. A.; Paul, K. E.; Jackman, R. J.; Whitesides, G. M. *Appl. Phys. Lett.* **1997**, *70*, 2658.
- Rogers, J. A.; Paul, K. E.; Jackman, R. J.; Whitesides, G. M. *J. Vac. Sci. Technol. B* **1998**, *16*, 59.
- Maria, J.; Malyarchuk, V.; White, J.; Rogers, J. A. *J. Vac. Sci. Technol. B* **2006**, *24*, 828.
- Smith, R. F.; Lorenz, K. T.; Ho, D.; Remington, B. A.; Hamza, A.; Rogers, J. A.; Pollaine, S.; Jeon, S.; Nam, Y. S.; Kilkenny, J. *Astrophys. Space Sci.* **2007**, *307*, 269.
- Talbot, H. F. *Philos. Mag.* **1836**, *9*, 401.
- Rayleigh, L. *Philos. Mag.* **1881**, *11*, 196.
- Berry, M.; Marzoli, I.; Schleich, W. *Phys. World* **2001**, *14*, 39.
- Latimer, P.; Crouse, R. F. *Appl. Opt.* **1992**, *31*, 80.
- Klein, M. V. *Optics*; Wiley: New York, 1970.
- Menard, E.; Bilhaut, L.; Zaumseil, J.; Rogers, J. A. *Langmuir* **2004**, *20*, 6871.
- Rolland, J. P.; Van Dam, R. M.; Schorzman, D. A.; Quake, S. R.; DeSimone, J. M. *J. Am. Chem. Soc.* **2004**, *126*, 2322.
- Rothrock, G. D.; Maynor, B.; Rolland, J. P.; DeSimone, J. M. *Proc. SPIE-Int. Soc. Opt. Eng.* **2006**, 6152.
- LaBianca, N.; Gelorme, J. D. *Proc. SPIE* **1995**, *2438*, 846.
- Teh, W. H.; Durig, U.; Drechsler, U.; Smith, G. C.; Guntherodt, H. J. *J. Appl. Phys.* **2005**, *97*, 054907.
- Kuebler, S. M.; Braun, K. L.; Zhou, W. H.; Cammack, J. K.; Yu, T. Y.; Ober, C. K.; Marder, S. R.; Perry, J. W. *J. Photochem. Photobiol. A-Chem.* **2003**, *158*, 163.
- Witzgall, G.; Vrijen, R.; Yablonovitch, E.; Doan, V.; Schwartz, B. *J. Opt. Lett.* **1998**, *23*, 1745.
- Lee, K. Y.; LaBianca, N.; Rishton, S. A.; Zolgharnain, S.; Gelorme, J. D.; Shaw, J.; Chang, T. H. P. *J. Vac. Sci. Technol. B* **1995**, *13*, 3012.
- Yang, S.; Megens, M.; Aizenberg, J.; Wiltzius, P.; Chaikin, P. M.; Russel, W. B. *Chem. Mater.* **2002**, *14*, 2831.
- Shaw, J. M.; Gelorme, J. D.; LaBianca, N. C.; Conley, W. E.; Holmes, S. J. *IBM J. Res. Dev.* **1997**, *41*, 81.
- Crivello, J. V. *J. Polym. Sci. A-Polym. Chem.* **1999**, *37*, 4241.
- Jun, Y. H.; Leatherdale, C. A.; Norris, D. J. *Adv. Mater.* **2005**, *17*, 1908.
- Kim, H. J.; Lee, J. K.; Kim, J. B.; Park, E. S.; Park, S. J.; Yoo, D. Y.; Yoon, D. Y. *J. Am. Chem. Soc.* **2001**, *123*, 12121.

- (76) Braun, P. V. Personal communication.
- (77) Dror, R.; Feigel, A. I.; Veinguer, M.; Sfez, B. G.; Klebanov, M.; Arsh, A.; Lyubin, V. *Proc. SPIE—Int. Soc. Opt. Eng.* **2005**, 5720, 56.
- (78) Wong, S.; Deubel, M.; Perez-Willard, F.; John, S.; Ozin, G. A.; Wegener, M.; Von Freymann, G. *Adv. Mater.* **2006**, 18, 265.
- (79) Denk, W.; Strickler, J. H.; Webb, W. W. *Science* **1990**, 248, 73.
- (80) Sun, H.-B.; Kawata, S. *Adv. Polym. Sci.* **2004**, 170, 169.
- (81) Kondo, T.; Matsuo, S.; Juodkazis, S.; Misawa, H. *Appl. Phys. Lett.* **2001**, 79, 725.
- (82) Shevchenko, E. V.; Talapin, D. V.; Kotov, N. A.; O'Brien, S.; Murray, C. B. *Nature* **2006**, 439, 55.
- (83) Park, S. H.; Xia, Y. N. *Langmuir* **1999**, 15, 266.
- (84) Suresh, S. *Science* **2001**, 292, 2447.
- (85) Ledermann, A.; Cademartiri, L.; Hermatschweiler, M.; Toninelli, C.; Ozin, G. A.; Wiersma, D. S.; Wegener, M.; Von Freymann, G. *Nature Mater.* **2006**, 5, 942.
- (86) Bitá, I.; Choi, T.; Walsh, M. E.; Smith, H. I.; Thomas, E. L. *Adv. Mater.* **2007**, 19, 1403.
- (87) Wang, X.; Xu, J.; Lee, J. C. W.; Pang, Y. K.; Tam, W. Y.; Chan, C. T.; Sheng, P. *Appl. Phys. Lett.* **2006**, 88, 051901.
- (88) Man, W. N.; Megens, M.; Steinhardt, P. J.; Chaikin, P. M. *Nature* **2005**, 436, 993.
- (89) Zoorob, M. E.; Charlton, M. D. B.; Parker, G. J.; Baumberg, J. J.; Netti, M. C. *Nature* **2000**, 404, 740.
- (90) Lu, L. H.; Ryu, K. S.; Liu, C. *J. MEM. Sys.* **2002**, 11, 462.
- (91) Thorsen, T.; Maerkl, S. J.; Quake, S. R. *Science* **2002**, 298, 580.
- (92) Liu, R. H.; Lenigk, R.; Druyor-Sanchez, R. L.; Yang, J.; Grodzinski, P. *Anal. Chem.* **2003**, 75, 1911.
- (93) Kakuta, M.; Bessoth, F. G.; Manz, A. *Chem. Rec.* **2001**, 1, 395.
- (94) Stroock, A. D.; Dertinger, S. K. W.; Ajdari, A.; Mezit, I.; Stone, H. A.; Whitesides, G. M. *Science* **2002**, 295, 647.
- (95) He, B.; Burke, B. J.; Zhang, X.; Zhang, R.; Regnier, F. E. *Anal. Chem.* **2001**, 73, 1942.
- (96) Kenis, P. J. A.; Ismagilov, R. F.; Whitesides, G. M. *Science* **1999**, 285, 83.
- (97) Bykov, V. P. *Sov. J. Quantum Electron* **1975**, 4, 861.
- (98) John, S. *Phys. Rev. Lett.* **1987**, 58, 2486.
- (99) Mekis, A.; Chen, J. C.; Kurland, I.; Fan, S. H.; Villeneuve, P. R.; Joannopoulos, J. D. *Phys. Rev. Lett.* **1996**, 77, 3787.
- (100) Chutinan, A.; Mochizuki, M.; Imada, M.; Noda, S. *Appl. Phys. Lett.* **2001**, 79, 2690.
- (101) Lin, S. Y.; Chow, E.; Bur, J.; Johnson, S. G.; Joannopoulos, J. D. *Opt. Lett.* **2002**, 27, 1400.
- (102) Xu, Y.; Lee, R. K.; Yariv, A. *J. Opt. Soc. Am. B—Opt. Phys.* **2000**, 17, 387.
- (103) Maldovan, M.; Thomas, E. L. *Nature Mater.* **2004**, 3, 593.
- (104) Toader, O.; Chan, T. Y. M.; John, S. *Phys. Rev. Lett.* **2004**, 92, 043905.
- (105) Qi, M. H.; Lidorikis, E.; Rakich, P. T.; Johnson, S. G.; Joannopoulos, J. D.; Ippen, E. P.; Smith, H. I. *Nature* **2004**, 429, 538.
- (106) Lin, S. Y.; Fleming, J. G.; Hetherington, D. L.; Smith, B. K.; Biswas, R.; Ho, K. M.; Sigalas, M. M.; Zubrzycki, W.; Kurtz, S. R.; Bur, J. *Nature* **1998**, 394, 251.
- (107) Blanco, A.; Chomski, E.; Grubtchak, S.; Ibisate, M.; John, S.; Leonard, S. W.; Lopez, C.; Meseguer, F.; Miguez, H.; Mondia, J. P.; Ozin, G. A.; Toader, O.; van Driel, H. M. *Nature* **2000**, 405, 437.
- (108) Garcia-Santamaria, F.; Lopez, C.; Meseguer, F.; Lopez-Tejiera, F.; Sanchez-Dehesa, J.; Miyazaki, H. T. *Appl. Phys. Lett.* **2001**, 79, 2309.
- (109) Gratson, G. M.; Garcia-Santamaria, F.; Lousse, V.; Xu, M. J.; Fan, S. H.; Lewis, J. A.; Braun, P. V. *Adv. Mater.* **2006**, 18, 461.
- (110) Pang, Y. K.; Lee, J. C. W.; Lee, H. F.; Tam, W. Y.; Chan, C. T.; Sheng, P. *Optics Express* **2005**, 13, 7615.